Research Square

Preprints are preliminary reports that have not undergone peer review.
They should not be considered conclusive, used to inform clinical practice,
or referenced by the media as validated information.

Engineering a Thermostable Ketone Amination Reductase from Aspergillus oryzae via Evolution-Based Design

Jiaying Wu
Huaqiao University
Chuxin Wang
Huaqiao University
Wenxuan Zhang
Huaqiao University
Siqi Xu
Huaqiao University
Ximan Huang
Huaqiao University
Li Wen
Huaqiao University
Peiqin Chen
Huaqiao University
Chunying Jin
Huaqiao University
Guangya Zhang
Huaqiao University
Wei Jiang
tianya416@126.com
Huaqiao University

Research Article

Keywords: Ancestral sequence reconstruction, Semi-rational design, Aspergillus oryzae, Thermostability Biocatalysis

Posted Date: July 22nd, 2026

DOI: https://doi.org/10.21203/rs.3.rs-10103914/v1

License: This work is licensed under a Creative Commons Attribution 4.0 International License.
Read Full License

Additional Declarations: No competing interests reported.

Abstract

Ancestral sequence reconstruction (ASR) is an effective semirational strategy for enzyme engineering that integrates evolutionary information with bioinformatic analysis. Here, ASR was combined with structure-guided mutagenesis using FuncLib and experimental validation to improve the catalytic performance and stability of the reductive aminase from *Asp*ergillus oryzae (*Asp*RedAm). Phylogenetic analysis of *Asp*RedAm and its homologs enabled the reconstruction of ancestral variants, including Anc43, Anc74, and Anc75, and guided the identification of key substrate-binding pockets and catalytically relevant residues. Targeted mutagenesis was then performed to generate improved variants. Among the resulting enzymes, Anc74_7 and Anc75_20 exhibited markedly enhanced catalytic activity and thermostability relative to *Asp*RedAm. In particular, their specific activities increased by up to 1.6- and 2.2-fold, respectively. Molecular docking together with kinetic analysis suggested that these improvements arose from active-site reconfiguration and an optimized substrate-binding microenvironment. Collectively, these results demonstrate the utility of integrating ASR with structure-guided engineering for the development of high-performance biocatalysts and provide insight into enzyme functional evolution and rational design.

Key points

1. ASR engineered RedAm variants with higher activity and thermostability.

2. Anc74_7 and Anc75_20 showed improved and catalytic efficiency (/).

3. Structural optimization enhanced AspRedAm stability, binding, and efficiency.

INTRODUCTION

Chiral amines are important nitrogen-containing motifs in pharmaceuticals, agrochemicals, and other bioactive molecules (Bai et al. 2026; Xia et al. 2025). They are widely found in natural products and functional compounds, where they often influence molecular recognition, potency, and selectivity(Tunç et al. 2025). Notably, about 40% of active pharmaceutical ingredients and 20% of agrochemicals contain chiral amine scaffolds (Cheng et al. 2025), underscoring their broad synthetic and industrial significance. In agrochemical applications, enantiomerically enriched chiral amines may also deliver higher efficacy at lower application rates than racemic analogues. Consequently, chiral amines are valuable building blocks and major targets in asymmetric synthesis (Zhu et al. 2026), and their growing demand continues to drive the development of efficient and selective production methods.

Industrial synthesis of chiral amines still depends largely on chemical catalysis, particularly asymmetric hydrogenation, asymmetric transfer hydrogenation, and racemate resolution(Gao et al. 2023; Li et al. 2024). Although these methods are well established, they often require harsh conditions and strict process control and may remain suboptimal in terms of sustainability(Takle et al. 2025), stereoselectivity, and cost-effectiveness (Vikhrankar et al. 2024). By contrast, biocatalysis has emerged

as an attractive alternative because it enables asymmetric transformations under mild conditions while providing high substrate specificity, excellent stereoselectivity, and products with high enantiomeric purity (Zhang et al. 2025b). Enzymes used for chiral amine synthesis include ω-transaminases(D. Patil et al. 2018; Zhang et al. 2025b), imine reductases, monoamine oxidases, amine dehydrogenases(Chen et al. 2025b; Shao et al. 2024), amino acid dehydrogenases(Zhou et al. 2024), and ketimine reductases (Chen et al. 2025a). However, their wider application is often limited by narrow substrate scope, low catalytic efficiency, poor compatibility with non-native substrates, restricted enzyme availability, or theoretical yield limitations. Thus, continued efforts in enzyme discovery, protein engineering, and process optimization are needed to expand the utility of biocatalytic routes to chiral amines.(Tseliou et al. 2024)

Among these enzymes, the reductive aminase from *Asp*ergillus oryzae (*Asp*RedAm)(Aleku et al. 2017) has attracted particular attention. *Asp*RedAm is an NADPH-dependent member of the imine reductase (IRED) superfamily and was the first eukaryotic IRED homolog to be identified (Ye et al. 2015). It catalyzes direct one-step asymmetric reductive amination of ketones with amines to furnish structurally diverse chiral amines and shows higher catalytic efficiency than many reported IREDs (Aleku 2017). In addition to reductive amination, *Asp*RedAm also catalyzes imine reduction and oxidative deamination, enabling its use in the kinetic resolution of racemic amines (Guo et al. 2025). The enzyme displays relatively broad substrate tolerance toward linear, cyclic, and preformed imine substrates, although it generally performs better with primary amines than with cyclic or secondary amines (Nielsen et al. 2025). Despite these advantages, *Asp*RedAm is strongly affected by pH and shows limited thermal stability, with substantial precipitation after incubation at 40 ℃ for about 1 h (Stillman et al. 1993). These drawbacks restrict its practical applicability and make improvement of its stability and catalytic performance an important engineering objective.

Because wild-type enzymes often do not meet the activity, stability, and productivity requirements of practical synthesis, protein engineering has become essential for developing robust biocatalysts (Mangas-Sanchez et al. 2017). Among current approaches, semirational design is especially attractive because it balances mutation diversity with screening efficiency (Ijäs 2019; Mousavi et al. 2025). By integrating sequence analysis, structural information, and computational modeling, this strategy can identify mutational hotspots affecting catalytic activity, substrate scope, or stability, thereby enabling focused library construction. Computational tools such as FoldX, PROSS, FuncLib, and FireProt further facilitate redesign by predicting mutational effects before experimental testing (Chica et al. 2005; Skolnick et al. 2025). Among semirational strategies, ancestral sequence reconstruction (ASR) has emerged as a powerful approach that combines evolutionary analysis with bioinformatics (Kuhlman and Bradley 2019; Santos et al. 2019). By inferring extinct ancestral proteins from phylogenetic relationships among extant homologs, ASR enables exploration of a relatively small but functionally enriched sequence space (Weng et al. 2025). Ancestral proteins frequently show enhanced thermostability, broader substrate tolerance, and diversified catalytic properties (Akanuma 2025), while requiring only limited experimental screening (Jermann et al. 1995; Prakinee et al. 2024; Stackhouse et al. 1990). These features make ASR particularly attractive for engineering *Asp*RedAm.

In this study, we combined ASR with structure-guided design and experimental validation to improve *Asp*RedAm. Phylogenetic analysis of *Asp*RedAm and its homologs enabled reconstruction of three ancestral enzymes, Anc43, Anc74, and Anc75. Molecular docking was then used to compare substrate-binding pockets and identify key active-site residues, leading to selection of nine candidate mutation sites. FuncLib-based semirational mutagenesis generated 50 variant models, of which the 20 top-ranked designs were experimentally evaluated. Among them, Anc74_7 and Anc75_20 showed improved catalytic activity and stability relative to *Asp*RedAm and the initial ancestral enzymes, with specific activities increased by 1.6- and 2.2-fold, respectively. These improvements were mainly associated with favorable active-site reorganization and an optimized substrate-binding microenvironment. Collectively, this work demonstrates the value of integrating ASR, computational design, and wet-lab screening for *Asp*RedAm engineering and provides a practical framework for developing more efficient reductive aminases. The main research content of this study is shown in Fig. 1.

MATERIALS AND METHODS

Construction of the ancestral sequence

A reductive aminase from *Aspergillus oryzae*, previously engineered in the laboratory and successfully expressed in *Escherichia coli*, was developed based on the structure and sequence of *Asp*RedAm (Q2TW47)(Aleku et al. 2017). This protein was employed as a query in BLAST searches against the NCBI protein database (https://www.ncbi.nlm.nih.gov/) to identify homologous sequences. Filtering criteria were applied to retain sequences exhibiting > 50% identity, > 90% query coverage, and lengths ranging between 290 and 300 amino acid residues.Ancestral sequences were reconstructed in PAMLX using CODEML with the selected evolutionary models. The curated multiple sequence alignment and phylogenetic tree were used as inputs. PAML implements maximum likelihood-based phylogenetic inference with diverse substitution models. Reconstructed internal-node sequences were extracted and evaluated, and three nodes, Anc43, Anc74, and Anc75, were selected for further analysis.

Identification of potential mutation sites

Structural alignment of *Asp*RedAm with three ancestral proteins gave RMSD values of < 2.0 Å, indicating high overall structural conservation. Residues within 4.0 Å of the substrate were defined as mutation candidates, whereas literature-reported catalytic residues were retained as conserved positions. Structural coordinates and site information were submitted to the FuncLib server for mutant design. Parameters including the maximum number of mutated sites per variant, position weight matrix threshold, and mutation energy range were optimized. Based on FuncLib energy and stability rankings, the top 20 variants from each category were selected, generating 80 candidates for experimental screening.

In Silico Screening and MD Simulation

Candidate mutants were evaluated based on structural stability, docking affinity, and predicted solubility. The 80 variants obtained from the initial screen were refined with FoldX, which was also used to estimate mutational effects on protein stability. Docking toward the carbonyl substrate, amine substrate, and NADPH was performed with AutoDock Vina, and variants were ranked by docking energy. Solubility was predicted using DeepPredict. The top 15 variants from the integrated ranking were subjected to molecular dynamics simulations. Protein–ligand complexes were parameterized, solvated, neutralized, minimized, and equilibrated before 10 ns production runs. Trajectories were analyzed using the free energy landscape (FEL) and related stability metrics. Three variants, Anc74_7, Anc75_8, and Anc75_20, were selected for experimental validation.

Expression and purification of mutants

Mutant plasmids were transformed into *E. coli* BL21(DE3). A single colony was cultured in 20 mL LB medium containing kanamycin (100 μg/mL) at 37 ℃ and 200 rpm for 12 h, and the culture was then inoculated (1:100, v/v) into 200 mL fresh medium. Cells were grown to an OD_{600} of 0.5–0.6 and induced with 200 μL of 0.1 M IPTG at 20 ℃ for 20 h. Cells were harvested by centrifugation, resuspended in precooled 0.1 M Tris–HCl buffer (pH 9.0), and disrupted by sonication on ice. After centrifugation, the supernatant was subjected to Ni^{2+} affinity chromatography, and His_6-tagged proteins were eluted with a 30–300 mM imidazole gradient in buffer containing 300 mM NaCl. Purified proteins were desalted and concentrated using a 10 kDa ultrafiltration membrane. Purity was analyzed by SDS-PAGE with Coomassie Brilliant Blue staining, and protein concentration was measured using a BCA assay kit (Beyotime).

Enzymatic Characterization

Enzyme activity was determined by monitoring NADPH/NADH consumption at 340 nm (ε = 6.22 mM^{-1} cm^{-1}). Unless otherwise noted, assays were performed in 200 μL of Tris–HCl buffer (pH 7.0) containing 10 mM carbonyl substrate, 20 mM amine substrate, 1 mM NADPH, and 0.5 mg/mL enzyme.

Optimum Temperature and pH

Optimum temperature was determined by preincubating cofactor-free reaction mixtures at 20–90 ℃ for 5 min, followed by activity measurement under standard conditions. Optimum pH was determined using cofactor-free systems at pH 3.0–10.0 after incubation at 30 ℃ for 5 min. The highest activity was set to 100%. All measurements were performed in triplicate.

Thermal and pH Stability

Cofactor-free enzyme samples were incubated at 30 or 50 ℃, and residual activity was measured after 1, 2, 4, 6, 9, 12, 24, 48, 96, 144, 216, 312, and 432 h. Initial activity was defined as 100%.

Organic Solvent Stability

Enzymes were incubated in cofactor-free reaction mixtures containing 10% (v/v) methanol, isopropanol, ethyl acetate, or DMSO for 150 min. Residual activity was measured every 30 min. The highest activity was set to 100%. All experiments were performed in triplicate.

Kinetic Analysis

1-indanone and propargylamine were used as substrates at concentration ranges of 0–10 and 0–20 mM, respectively. Reactions were performed under the respective optimal temperature and pH conditions. Kinetic parameters were obtained by fitting the data to the Michaelis–Menten model.

Molecular docking

Protein structures were refined with FoldX and energy-minimized in GROMACS. The lowest-energy structure was used for docking. Substrate and cofactor structures were obtained from PubChem and prepared together with the receptor in AutoDock tools 1.5.7 by removing water molecules and adding hydrogen atoms. Docking was performed with AutoDock_Vina 1.2.5 using a 25 × 25 × 25 $Å^3$ grid box, an energy range of 4 kcal/mol, and an exhaustiveness of 8. Ten poses were generated, and the lowest-energy conformation was selected for further analysis.

Molecular Dynamics Simulation

MD simulations were performed in GROMACS to evaluate the stability of *Asp*RedAm, Anc74_7, Anc75_8, and Anc75_20. The CHARMM36 force field was used for all systems. Each protein–ligand complex was centered in a cubic box with a 1.5 nm buffer, solvated with TIP3P water, and neutralized with Na^+/Cl^- ions under periodic boundary conditions. After energy minimization using the steepest descent and conjugate gradient methods, the systems were equilibrated at 30 ℃ under NVT and NPT conditions. Production simulations were then run for 100 ns, and stability and compactness were analyzed using free energy landscape (FEL) analysis.

RESULT And DISCUSSION

Ancestral sequence reconstruction

A comprehensive phylogenetic analysis was performed to elucidate the evolutionary relationships among *Asp*RedAm and its homologous sequences, providing a framework for subsequent ancestral sequence reconstruction. Experimentally validated *Asp*RedAm sequences were employed as references to retrieve 41 homologous sequences from the National Center for Biotechnology Information (NCBI) database (https://www.ncbi.nlm.nih.gov/). Sequences that compromised alignment quality were manually excluded, and non-conserved regions were corrected to ensure accurate multiple sequence alignment. An agglomerative approach was subsequently used to construct a phylogenetic tree, which was visualized via iTOL (https://itol.embl.de/) (Gupta et al. 2024) **(Figure S1)**. Distinct evolutionary

clustering among the sequences was observed, establishing a structural basis for identifying key ancestral nodes and guiding the selection of candidate sequences for functional characterization.

To investigate the sequence-function relationship within the *Asp*RedAm family, ancestral sequence reconstruction (ASR) was employed as an evolution-directed strategy. This method infers ancestral protein sequences from phylogenetic relationships using probabilistic models and has been widely applied to generate enzymes with enhanced thermal stability and expanded functional repertoire (Benner et al. 2007; Jiao and Jiang 2023). ASR enables the exploration of extinct sequence space and provides a robust framework for interpreting functional diversification among homologous proteins. The procedure involves constructing a phylogenetic tree from multiple sequence alignments of homologous proteins and inferring the amino acid sequences of ancestral nodes(Liu et al. 2026; Orrego et al. 2021). In this study, ancestral sequences of *Asp*RedAm and its homologues were inferred using the maximum likelihood approach. Prior studies indicate that the position of ancestral nodes within a phylogenetic tree significantly influences protein structure and function: peripheral nodes are frequently associated with functional diversification, whereas central nodes generally confer higher structural stability. Based on these principles, three ancestral nodes — Anc43, Anc74, and Anc75 — exhibiting substantial sequence divergence and peripheral positions in the phylogenetic tree were selected for detailed analysis **(**Fig. 2**).**

Mutation design using the FuncLib online server

Molecular docking analysis was used to identify the substrate-binding pockets and key residues of *Asp*RedAm and its three ancestral enzymes **(Figure S2)**. Based on this information, nine potential mutation sites were identified for *Asp*RedAm, Anc43, Anc74 and Anc75. Semi-rational mutation designs were then performed on these sites using the FuncLib online server (http://FuncLib.weizmann.ac.il/) (Gasteiger et al. 2005). As an automated enzyme design method, FuncLib combines evolutionary conservation analysis with Rosetta atomic-level modelling to rapidly construct libraries of enzyme variants that are highly stable and exhibit excellent catalytic performance and diverse functions, eliminating the need for high-throughput screening. This significantly shortens the enzyme engineering R&D cycle and reduces experimental costs, making it of great practical value and broad significance (Yao et al. 2021). Mutation design schemes were generated for each of the four enzymes — *Asp*RedAm, Anc43, Anc74 and Anc75 — with 50 variant structures generated for each enzyme. The 200 highest-scoring mutants were then selected from each set of 50, yielding a total of 80 potentially beneficial mutants for subsequent structural analysis and experimental validation.

Multifactorial screening of mutants

FoldX is an empirical force-field-based computational tool widely used to estimate the effects of amino acid substitutions on protein stability. Owing to its relatively high success rate in identifying destabilizing mutations, FoldX is well suited for the preliminary screening of mutant libraries. Although the predictions of FoldX are subject to certain errors, their reliability can be improved by integrating molecular dynamics simulations(Chen et al. 2024a). Accordingly, variants with predicted stability changes (△△G) below − 12 kcal/mol were retained for further analysis.DeepPredict is a protein structure prediction web server that

integrates the Porter6(Ho et al. 2025) and PaleAle6(Liu et al. 2024) models. By leveraging deep learning, it enables accurate prediction of protein secondary structure and relative solvent accessibility (RSA). Notably, this approach captures both local sequence patterns and long-range dependencies without relying on multiple sequence alignment (MSA), thereby improving prediction accuracy while maintaining computational efficiency.In this study, 15 variants were selected for further analysis based on three criteria: predicted stability change (△△G) of less than − 16.3.24 kcal/mol as calculated by FoldX **(**Fig. 3a**)**, docking binding energy of less than − 12 kcal/mol as estimated by AutoDock Vina **(**Fig. 3b**)**, and relative solvent accessibility (RSA) greater than 0.571 (Fig. 3c).

Note

Performance evaluation of mutants was conducted through three *Asp*ects: stability(a), docking binding energy(b), and solubility(c).

Molecular dynamics (MD) simulations were performed for 10 ns at 30 ℃ on the protein-ligand complexes of the 15 selected variants, followed by the construction of free energy landscapes (FELs). An FEL represents the distribution of free energy by projecting MD trajectories onto a low-dimensional conformational space, thereby providing insights into the conformational distribution and stability of enzyme-ligand complexes. Compared with single-parameter metrics such as root-mean-square deviation (RMSD) or root-mean-square fluctuation (RMSF), FEL analysis offers a more comprehensive view of the system's conformational sampling in terms of energy distribution, enabling identification of predominant conformational states and their energetic characteristics during simulation.Comparison of the FELs across the 15 complexes **(Figure S3)** revealed notable differences in free energy distribution patterns. Certain complexes exhibited a single, deep, and concentrated low-energy basin, indicating that the complex predominantly adopted a stable conformation throughout the simulation. In contrast, other complexes displayed multiple low-energy basins or broad low-energy regions, reflecting the presence of metastable states or conformational transitions, and suggesting higher flexibility and reduced stability. Based on these analyses, three variants — Anc74_7, Anc75_8, and Anc75_20 — were selected for further experimental validation, as they exhibited distinct low-energy regions, well-defined primary energy valleys, and relatively sharp basin boundaries.

Analysis of the Enzymatic Properties of the Mutants

Optimal temperature and pH of AspRedAm and variants

Consistent with the high-confidence structural predictions described above, the selected ancestral enzymes Anc43, Anc74, and Anc75 were successfully expressed in soluble form and purified via Ni2+–NTA affinity chromatography. SDS-PAGE analysis revealed single, well-defined bands corresponding to the expected molecular mass of approximately 30.3 kDa, as predicted by Expasy ProtParam **(Figure S4)**. These results confirm the structural integrity and homogeneity of the purified ancestral enzymes, thereby providing a reliable basis for subsequent enzymatic characterisation

Given the broad substrate scope and favorable catalytic performance of the variants, their optimal reaction temperature and pH were systematically evaluated to define suitable catalytic conditions. As shown in **Figure S5a**, the three mutants exhibited similar temperature-activity profiles and shared an optimal reaction temperature of 50 ℃ with the ancestral enzyme. In all three variants, relative activity increased progressively with temperature, reached a maximum at 50 ℃, and then declined gradually at higher temperatures. Notably, the mutants retained approximately 60% of their relative activity at 80–90 ℃, indicating substantial thermotolerance and improved high-temperature performance relative to the ancestral enzyme. **Figure S5b** illustrates the pH-activity profiles of the mutants. The enzymatic activity of all three variants increased progressively with rising pH, reaching a maximum at pH 7, indicating that their optimal catalytic environment is near-neutral. Beyond pH 7, activity declined gradually; however, the mutants retained approximately 50% of their relative activity under strongly alkaline conditions (pH 10), demonstrating a notable degree of alkaline tolerance while preserving the ancestral enzyme's preference for near-neutral conditions.

Half-lives of AspRedAm and its variants

Because the ancestral-derived variants exhibited improved substrate specificity and markedly enhanced catalytic activity, their half-lives were evaluated to assess whether gains in activity were accompanied by reduced stability. At 30 ℃ **(**Fig. 4a**)**, the relative activities of the three mutants declined gradually over time. After approximately 216 h, the rate of decline accelerated, and activity decreased to 50% of the initial level at around 840 h, corresponding to the half-life. Although the mutants were slightly less stable than the ancestral enzyme, they remained substantially more stable than *Asp*RedAm, with half-lives that were approximately 187-fold longer, indicating markedly improved long-term stability.At 50 ℃ **(**Fig. 4b**)**, the three mutants also retained favorable thermal stability. Anc74_7 and Anc75_20 reached 50% relative activity after approximately 264 h; although this was somewhat shorter than that of the ancestral enzyme, their half-lives were still approximately 377-fold longer than that of *Asp*RedAm. Anc75_8 exhibited a half-life of approximately 312 h, which was comparable to that of the ancestral enzyme, further confirming its strong thermal tolerance. Collectively, these results indicate that the mutation and screening strategy enhanced catalytic performance without substantially compromising overall stability, supporting its potential for long-term biocatalysis and industrial application.

Note

(a) Half-life of *Asp*RedAm and variants at 30℃; Figure (b) Half-life of *Asp*RedAm and variants at 50℃

Stability of AspRedAm and its variants in organic solvents

Because organic solvents are often unavoidable in industrial processes, evaluating enzyme stability in such environments is essential for assessing industrial applicability. On the basis that the three mutants had already shown good thermal and pH stability, their catalytic performance was further examined in the presence of common organic solvents. As shown in **Figure S6**, the parental enzyme system was used to assess four industrially relevant solvents: methanol, isopropanol, ethyl acetate, and dimethyl

sulfoxide (DMSO). Under these conditions, all three mutants exhibited strong solvent tolerance, with residual activities significantly higher than that of wild-type *Asp*RedAm and, in most cases, higher than those of the corresponding ancestral enzymes. These results indicate improved solvent adaptability.Specifically, after 150 min of incubation in 10% (v/v) methanol or DMSO **(Figure S6a and d)**, the residual activities of all three mutants remained at approximately 80%, indicating robust tolerance to polar solvents. Although activity decreased in isopropanol **(Figure S6b)** and ethyl acetate **(Figure S6c)**, it still remained above 50% and 60%, respectively, after 150 min of incubation, suggesting that the mutants also retained appreciable stability in moderately or weakly polar solvents. Collectively, these findings show that the mutant enzymes were substantially more stable in organic solvent systems than *Asp*RedAm and, in some cases, even outperformed the ancestral enzymes, supporting their improved environmental adaptability and potential for industrial biocatalysis in solvent-containing systems.

Determination of enzyme activity for AspRedAm and its ancestral variants

Enzyme activity in this study was defined as the amount of enzyme required to catalyze the consumption or production of 1 μmol of NADPH per minute under specified reaction conditions. Activity was quantified using the following formula:

Enzyme activity (U)=[$\triangle A_{340} \times V_{total}$(mL)×$10^3$×Dilution factor] / [ε340 NADPH×l×min]

where A_{340} represents the change in absorbance at 340 nm, V_{total} is the total reaction volume (mL), ε340 NADPH is the molar extinction coefficient of NADPH at 340 nm, and l is the optical path length.

As shown in Fig. 5, all three mutants exhibited significantly higher specific activity compared with the parental enzyme ($p < 0.01$), indicating that the applied mutation strategy effectively enhanced catalytic performance. Among the variants, Anc74_7 displayed the highest activity. Although Anc75_8 showed slightly lower activity than the other two mutants, its catalytic level remained approximately fourfold higher than that of *Asp*RedAm, demonstrating substantial overall improvement. These results validate the effectiveness of the previous mutation design and screening strategy. The observed enhancement in enzyme activity may be attributed to improved enzyme-substrate interactions, potentially through optimization of the active site conformation or refinement of the substrate-binding microenvironment, thereby increasing overall catalytic efficiency.

Kinetic studies of variants

To determine whether the improvements in stability and catalytic activity of the variants were accompanied by changes in catalytic behavior, steady-state kinetic parameters were systematically measured using representative substrates. The results are summarized in Tables 1 and 2. 1-indanone was used as the carbonyl donor for kinetic analysis (Table 1). Compared with *Asp*RedAm, all three mutants exhibited markedly higher K_{cat} values and lower K_m values, indicating improved substrate affinity and faster catalytic turnover. As a result, their catalytic efficiencies (K_{cat}/K_m) increased by more than 1.7-fold relative to *Asp*RedAm, with Anc75_20 showing an increase of more than 2-fold. In addition,

these variants further outperformed the previously constructed ancestral enzyme in catalytic efficiency, indicating that the introduced mutations at key residues exerted a positive effect on catalytic performance.When cyclohexylamine was used as the amine donor (Table 2), the K_m values of the three mutants were slightly higher than that of *Asp*RedAm, suggesting modest differences in substrate affinity. However, their K_{cat} values were more than twice that of *Asp*RedAm. These findings suggest that the mutation strategy enhanced overall catalytic performance primarily by increasing turnover rate, thereby offsetting changes in substrate binding. Overall, the rational design and directed optimization of the ancestral enzyme not only improved stability but also significantly enhanced kinetic performance. These results demonstrate that catalytic efficiency can be effectively increased without compromising structural stability, providing useful guidance for the engineering of high-performance biocatalysts.

Table 1
Kinetic Parameters of *Asp*RedAm and Its variants

***Asp*RedAm**	**K_m(μmol/L)**	**K_{cat} (s^{-1})**	**K_{cat}/K_m(S^{-1}μmol/L^{-1})**
	1.695 ± 0.219	**279.3 ± 7.5**	**164.8 ± 21.8**
Anc74_7	1.38 ± 0.10	391.83 ± 8.66	283.9 ± 21.5
Anc75_8	1.35 ± 0.11	422.84 ± 10.50	313.2 ± 26.7
Anc75_20	1.22 ± 0.08	391.63 ± 6.83	360 ± 23.6

Table 2
Kinetic Parameters of *Asp*RedAm and Its variants

***Asp*RedAm**	**K_m(μmol/L)**	**K_{cat} (s^{-1})**	**K_{cat}/K_m(S^{-1}μmol/L^{-1})**
	1.563 + 0.212	**182.4 ± 4.3**	**116.7 ± 16.1**
Anc74_7	1.70 + 0.18	389.48 + 9.81	229.1 ± 24.9
Anc75_8	1.66 + 0.16	387.43 + 8.71	233.4 ± 23.1
Anc75_20	1.51 + 0.12	378.60 + 6.80	250.7 ± 20.4

Mechanistic analysis of the increased activity and stability of the mutants

Molecular docking analysis of the mutants

As shown in the molecular docking results (Fig. 6), the key difference between *Asp*RedAm (Fig. 6a) and the mutants Anc74_7 (Fig. 6b), Anc75_8 (Fig. 6c), and Anc75_20 (Fig. 6d) lies in the formation of more stable hydrogen-bond interactions between the ligand and residues in the active site. This provides an important structural basis for the improved catalytic performance of the mutants.In Anc74_7, additional direct hydrogen bonds were observed between the ligand and key residues such as Asp280 and Ser235.

These hydrogen-bond distances were mainly within 2–3 Å, indicating tighter and more stable ligand binding. In Anc75_8 and Anc75_20, the number of residues involved in ligand interactions increased further. For example, Ala120, Gly153, and Ser155 formed a cooperative multi-site interaction network, allowing the ligand to adopt a more stable and constrained binding conformation in the active site. Such a hydrogen-bond network enhances substrate anchoring, improves binding affinity and positional accuracy, and helps maintain the reactive group in a geometry more favorable for catalysis.

Note

(a) Molecular docking analysis of *Asp*RedAm; (b) Molecular docking analysis of Anc74_4; (c) Molecular docking analysis of Anc75_8; (d) Molecular docking analysis of Anc75_20

Molecular dynamics simulations of mutants

Molecular dynamics simulations were conducted on the Anc74_7, Anc75_8, and Anc75_20 protein–ligand complexes for 100 ns at 303 K. The results are shown in Fig. 7.As shown in the RMSD profiles **(**Fig. 7a**)**, the three variants reached equilibrium more rapidly than *Asp*RedAm and displayed smaller fluctuations throughout the simulation(Hernández-Meléndez et al. 2025). This indicates greater structural stability and reduced conformational drift under thermal motion, further supporting the effectiveness of ancestral sequence reconstruction combined with semi-rational design in generating more stable *Asp*RedAm variants.The radius of gyration (Rg) results also support this conclusion(Qiu et al. 2025) **(**Fig. 7b**)**. Compared with *Asp*RedAm, the variants exhibited lower and more stable Rg values, suggesting a more compact protein core. Such compaction likely increases structural rigidity and contributes to enhanced stability.The solvent-accessible surface area (SASA) reflects the extent of solvent exposure of the ligand over time **(**Fig. 7c**)**. Compared with the three variants, *Asp*RedAm showed slightly higher SASA values, indicating a looser molecular packing and a less compact binding environment(Wang et al. 2024). In contrast, the lower SASA values of the variants suggest tighter encapsulation of the ligand, consistent with their improved structural stability.

Note

(a) RMSD analysis of *Asp*RedAm and variants; (b) Rg analysis of *Asp*RedAm and variants; (c) SASA analysis of *Asp*RedAm and variants.

Analysis of the free energy landscape for mutants

Free energy landscapes (FELs) were constructed based on principal component analysis of the molecular dynamics trajectories(Zhu et al. 2025). As shown in **Figure S7**, the conformational distributions and energy convergence patterns of the different systems in principal component space differed markedly.For *Asp*RedAm **(Figure S7a)**, the low-free-energy region is relatively narrow and elongated, indicating that although the system reaches a low-energy state, the corresponding conformational states are dispersed and remain associated with pronounced spatial fluctuations,

suggesting limited overall stability(Kalpokas et al. 2025). In contrast, the three variants **(Figure S7b–d)** display more concentrated low-free-energy basins, more uniform conformational distributions, and smaller fluctuations. In addition, the well-defined basin boundaries and high peripheral energy barriers restrict transitions to unfavorable conformations, indicating that the mutant protein - ligand complexes more effectively stabilize the key enzymatic conformations(Scherer et al. 2025; Zhang et al. 2025a).Among them, Anc75_8 exhibits the most distinct localized low-energy basin with high energy density and pronounced surrounding barriers. This suggests that once the system adopts this dominant conformation, the likelihood of transitioning to alternative conformations is low.(Chen et al. 2024b) Taken together, these features indicate superior stability from both kinetic and thermodynamic perspectives, highlighting Anc75_8 as the variant with the most pronounced stability advantage

Analysis of residual energy contributions in mutants

The residue-level free energy contribution analysis indicates that Anc74_7, Anc75_8, and Anc75_20 all exhibit more favorable energy distribution patterns than *Asp*RedAm(Koenekoop et al. 2025; Yeh and Hayes 2025) **(**Fig. 8**)**. Specifically, these variants show increased negative free energy contributions at key residues,(Zheng et al. 2025) whereas locally unfavorable positive contributions are markedly reduced. Combined with the molecular docking results and other analyses, this stabilizing effect appears to be concentrated mainly within the active pocket and its adjacent regions, suggesting a more favorable thermodynamic basis for substrate binding and maintenance of the catalytic conformation(Zarifi et al. 2025). In contrast, *Asp*RedAm displays several distinct positive free energy peaks **(**Fig. 8a**)**, particularly at V70 and S210. These residues contribute substantial positive free energy, which may hinder stable substrate binding and transition-state formation. By comparison, the three mutants have effectively optimized the active-site microenvironment through key residue substitutions and local structural remodeling **(**Fig. 8b **- d)**, thereby improving substrate binding modes and stabilizing the catalytic conformation.

Note

(a) Residue energy contribution analysis of *Asp*RedAm; (b) Residue energy contribution analysis of Anc74_7; (c) Residue energy contribution analysis of Anc75_8; (d) Residue energy contribution analysis of Anc75_20

Analysis of surface zeta potentials of mutants

Surface zeta potential analysis was performed for *Asp*RedAm and the three variants **(Figure S8)**. Compared with *Asp*RedAm, variants Anc74_7, Anc75_8, and Anc75_20 exhibit a more uniform surface charge distribution, with markedly reduced regions of extreme positive and negative potential. In the ligand-binding regions, these mutants also display improved charge complementarity, which is favorable for substrate recognition and stable binding. Such a more balanced electrostatic surface environment is expected to enhance environmental adaptability.On the one hand, a more homogeneous charge

distribution can reduce disturbances to local interaction networks caused by protonation changes, thereby improving tolerance to pH fluctuations(Ni et al. 2025). On the other hand, the reduction of highly charged surface patches may lessen dependence on the stabilizing effects of the hydration layer, decreasing susceptibility to surface-charge perturbations and the conformational instability they may induce in organic solvents or in the presence of metal ions. Accordingly, the three variants showed superior pH tolerance, organic solvent resistance, and ion tolerance, consistent with the enzymatic characterization results reported above.

DISCUSSION

This study demonstrates that the integration of ancestral sequence reconstruction (ASR) with semi-rational enzyme engineering represents an effective approach for systematically improving enzymatic performance. Using FuncLib-guided mutagenesis, followed by experimental validation and mechanistic analysis, we identified enzyme variants with substantially enhanced catalytic properties and stability compared to *Asp*RedAm. Variants Anc74_7 and Anc75_20 exhibited significant improvements in apparent catalytic efficiency and substrate affinity. Detailed mechanistic investigations revealed that these gains stemmed from active-site conformational optimization, the establishment of a more favorable substrate-binding microenvironment, enhanced negative free-energy contributions within the active pocket, reduced unfavorable positive energy contributions, and refined surface electrostatic properties. Collectively, these findings provide structural and thermodynamic insights into the observed functional enhancements, highlighting the utility of combining ASR with semi-rational design in enzyme engineering. This study also establishes a versatile framework for developing high-performance biocatalysts, offering a broadly applicable strategy for advancing enzyme engineering across diverse applications, including industrial biotechnology and biomedicine.

Declarations

ASSOCIATED CONTENT

Supporting Information.

The Supporting Information is available free of charge at:

Protein sequences as used herein; Phylogenetic Tree; Molecular Docking Analysis of *Asp*RedAm and Ancestral Sequences; Free Energy Landscape (FEL) of Mutants at 303 K; Optimal Temperature and pH of *Asp*RedAm and variants; Free energy landscape analysis of *Asp*RedAm and variants; Surface electrostatic potential analysis of *Asp*RedAm and ancestral sequence variants

AUTHOR INFORMATION

Corresponding Author

*Wei Jiang – College of Chemical Engineering, Huaqiao University, Xiamen 361021 Fujian Province, PR China; Email: tianya416@126.com

Author Contributions

Jiaying Wu, Chuxin Wang, Wenxuan, Zhang, Siqi Xu, Ximan Huang, Li Wen, Peiqin Chen, Chunying Jin – College of Chemical Engineering, Huaqiao University, Xiamen 361021 Fujian Province, PR China;

Guangya Zhang – Department of Bioengineering and Biotechnology, Huaqiao University, Xiamen 361021 Fujian Province, PR China.

Funding Sources

This work was supported by the National Natural Science Foundation of China [grant numbers 21808073]; Nanping City Science & Technology Program of China [grant numbers N2024K005], Natural Science Foundation of Fujian Province [grant numbers 2021J05058], the Fundamental Research Funds for the Central Universities [grant numbers ZQN-814], the high-levelpersonnel activation fee of Huaqiao University [grant numbers 600005-Z17Y0072], and Quanzhou City Science & Technology Program of China [grant numbers 2018C008].

Ethical Approval

Not applicable – this study did not involve human participants or animals.

Availability of data and materials

Not applicable – no datasets were generated or analysed during the current study.

Competing Interests

The authors declare no financial or personal conflicts of interest that could influence the work reported in this study. All experimental results, analyses, and interpretations were conducted objectively and transparently. Furthermore, the authors have no affiliations or involvement with any organization or entity that has a financial interest in the findings of this research.

References

1. Akanuma S (2025) Learning about protein stability and functional activity from ancestral reconstruction. J Mol Biol :169435
2. Aleku GA (2017) Development of Imine Reductases and Reductive Aminases for Chiral Amine Synthesis. The University of Manchester. (United Kingdom)
3. Aleku GA, France SP, Man H, Mangas-Sanchez J, Montgomery SL, Sharma M, Leipold F, Hussain S, Grogan G, Turner NJ (2017) A reductive aminase from Aspergillus oryzae. Nat Chem 9(10):961–969

4. Bai H, Li M, Wang X, Jiang T, Zeng L, Zhang L, Wang C (2026) Stereodivergent synthesis of chiral amines bearing vicinal stereocenters via hydroamination of trisubstituted alkenes. Nature Communications
5. Benner SA, Sassi SO, Gaucher EA (2007) Molecular paleoscience: systems biology from the past. Adv Enzymol Relat Areas Mol Biology 75:1
6. Chen B, Li R, Feng J, Zhao B, Zhang J, Yu J, Xu Y, Xing Z, Zhao Y, Wang B (2024a) Modular access to chiral amines via imine reductase-based photoenzymatic catalysis. J Am Chem Soc 146(20):14278–14286
7. Chen L, Fan W, Liu X, Fang Y, Zhu J (2025a) Asymmetric Reductive Amination of Structurally Diverse Ketones with an Engineered Amine Dehydrogenase. The Journal of Organic Chemistry
8. Chen Q, Wu J, Wu Y, Wang Z, Zeng M, He Z, Chen J, Mu W (2024b) Rational design of loop dynamics for a barrel-shaped enzyme by introducing disulfide bonds. J Agric Food Chem 72(24):13856–13868
9. Chen X-R, Jin T, Zhang C, Zhu Z-Y, Shen X-Y, Chen Q, Wang J, Xu J-H, Zheng G-W (2025b) Engineering an imine reductase for enhanced activity and reduced substrate inhibition: Asymmetric synthesis of chiral 2-aryl pyrrolidines. Chin J Catal 78:144–155
10. Cheng F, Zhou Y-L, Yang D-C, Zhao D-Y, Xue Y-P, Zheng Y-G (2025) Advances in biosynthesis of chiral amide herbicides and the key enzymes: dimethenamid-P and S-metolachlor as case studies. Bioresources Bioprocess 12(1):17
11. Chica RA, Doucet N, Pelletier JN (2005) Semi-rational approaches to engineering enzyme activity: combining the benefits of directed evolution and rational design. Curr Opin Biotechnol 16(4):378–384
12. Patil D, Grogan M, Bommarius G, Yun A H (2018) Recent advances in ω-transaminase-mediated biocatalysis for the enantioselective synthesis of chiral amines. Catalysts 8(7):254
13. Gao Y, Wang Z, Zhang X, Zhao M, Zhang S, Wang C, Xu L, Li P (2023) Additive-Free Transfer Hydrogenative Direct Asymmetric Reductive Amination Using a Chiral Pyridine-Derived Half-Sandwich Catalyst. Angew Chem 135(31):e202303709
14. Gasteiger E, Hoogland C, Gattiker A, Duvaud Se, Wilkins MR, Appel RD, Bairoch A (2005) Protein identification and analysis tools on the ExPASy server The proteomics protocols handbook. Springer, pp 571–607
15. Guo T, Zeng L, Liu J, Zhang X, Bai Y (2025) Phase-Separated Multienzyme Condensates for Efficient Synthesis of Imines from Carboxylic Acids with Enhanced Dual-Cofactor Recycling. Int J Mol Sci 26(10):4795
16. Gupta RK, Patel SK, Lee J-K (2024) Novel cofactor regeneration-based magnetic metal–organic framework for cascade enzymatic conversion of biomass-derived bioethanol to acetoin. Bioresour Technol 408:131175
17. Hernández-Meléndez JR, Paton AE, Perkins JC, Yang D, Chiang C-H, Narayan AR (2025) Ancestral Sequence Reconstruction to Accelerate Non-heme Iron-dependent Biocatalyst Engineering. ACS Cent Sci 11(11):2196–2205

18. Ho OM, Hoang T, Lee C (2025) Aromatic Residue F443 Modulates the Dimer Interface and Activity of Pseudomonas mandelii Glutathione Reductase. ACS omega 10(8):8709–8717
19. Ijäs T (2019) Design methodologies and the limits of the engineering-dominated conception of synthetic biology. Acta Biotheor 67(1):1–18
20. Jermann TM, Opitz JG, Stackhouse J, Benner SA (1995) Reconstructing the evolutionary history of the artiodactyl ribonuclease superfamily. Nature 374(6517):57–59
21. Jiao L, Jiang H-L (2023) Metal-organic frameworks for catalysis: Fundamentals and future prospects. Chin J Catal 45:1–5
22. Kalpokas A, Mackey M, Michel J (2025) Accurate Prediction of Drug Resistance for Intrinsically Disordered Protein Regions. J Chem Theory Comput 21(24):12497–12507
23. Koenekoop L, van de Brug N, Jespers W, Åqvist J, Gutiérrez-de-Terán H (2025) Accurate predictions of protein mutational effects accelerated with a hybrid-topology free energy protocol. Commun Chem 8(1):362
24. Kuhlman B, Bradley P (2019) Advances in protein structure prediction and design. Nat Rev Mol Cell Biol 20(11):681–697
25. Li B, Zhou G, Zhang D, Yao L, Li M, Yang G, Zhang S, Nie H (2024) Spiro-Josiphos ligands for the Ir-catalyzed asymmetric synthesis of chiral amines under hydrogenation conditions. Org Lett 26(10):2097–2102
26. Liu S, Deng P, Chen Q, Sun Q, Wang Y, Shi H, Liang K (2026) Reticular Chemistry: A Versatile Platform for Engineering Heterogenous Biocatalysts. Adv Sci 13(4):e19207
27. Liu Y, Qu W, Liu Y, Feng Y, Ma H, Tuly JA (2024) Assessment of cell wall degrading enzymes by molecular docking and dynamics simulations: Effects of novel infrared treatment. Int J Biol Macromol 258:128825
28. Mangas-Sanchez J, France SP, Montgomery SL, Aleku GA, Man H, Sharma M, Ramsden JI, Grogan G, Turner NJ (2017) Imine reductases (IREDs). Curr Opin Chem Biol 37:19–25
29. Mousavi N, Zhou E, Razavi A, Ebrahimi E, Varela-Castillo P, Yang X-J (2025) P3 site-directed mutagenesis: An efficient method based on primer pairs with 3'-overhangs. J Biol Chem 301(3):108219
30. Ni B, Fu Z, Zhao J, Yao X, Li W, Li X, Sun B (2025) Characterization and mechanism study of a novel ethanol acetyltransferase from Hanseniaspora uvarum (EatH) with good thermostability, pH stability, and broad alcohol substrate specificity. J Agric Food Chem 73(11):6828–6841
31. Nielsen JR, Kennerley J, Huang WE (2025) Directed evolution of hydrocarbon-producing enzymes. Biotechnol Biofuels Bioprod 18(1):91
32. Orrego AH, Andrés-Sanz D, Velasco-Lozano S, Sanchez-Costa M, Berenguer J, Guisan JM, Rocha-Martin J, López-Gallego F (2021) Self-sufficient asymmetric reduction of β-ketoesters catalysed by a novel and robust thermophilic alcohol dehydrogenase co-immobilised with NADH. Catal Sci Technol 11(9):3217–3230

33. Prakinee K, Phaisan S, Kongjaroon S, Chaiyen P (2024) Ancestral sequence reconstruction for designing biocatalysts and investigating their functional mechanisms. JACS Au 4(12):4571–4591
34. Qiu W, Yang P, Ye J, Zhou J, Liu S (2025) Unveiling highly active and stable l-glutaminase through ancestral sequence reconstruction and turnover number prediction. J Agric Food Chem 73(9):5353–5362
35. Santos YLdl, Chew-Fajardo YL, Brault G, Doucet N (2019) Dissecting the evolvability landscape of the CalB active site toward aromatic substrates. Sci Rep 9(1):15588
36. Scherer M, Kriegel M, Höcker B, Fleishman SJ (2025) Optimizing stability in dynamic small-molecule binding proteins. Journal of the American Chemical Society
37. Shao Y, Gao Y-D, He Z-L, Yang L-C (2024) Application of monoamine oxidase in organic synthesis. Chem Catal 4(10)
38. Skolnick J, Srinivasan B, Zhou H (2025) GlueFinder: A Data-Driven Framework for the Rational Discovery of Molecular Glues. bioRxiv:2025.10. 17.683126
39. Stackhouse J, Presnell SR, McGeehan GM, Nambiar KP, Benner SA (1990) The ribonuclease from an extinct bovid ruminant. FEBS Lett 262(1):104–106
40. Stillman T, Baker P, Britton K, Rice D (1993) Conformational flexibility in glutamate dehydrogenase: role of water in substrate recognition and catalysis. J Mol Biol 234(4):1131–1139
41. Takle MJ, Maurer DM, Staehle P, Dickhaut J, Holtze C, Hellgardt K, Hii KKM (2025) Scalable and sustainable synthesis of chiral amines by biocatalysis. Communications Chemistry
42. Tseliou V, Masman MF, Knaus T, Mutti FG (2024) Current status of amine dehydrogenases: from active site architecture to diverse applications across a broad substrate spectrum. ChemCatChem 16(24):e202400469
43. Tunç T, Kılınç N, Demirel N, Alım Z (2025) Chiral Anthranilic Amides as Potential Cholinesterase Inhibitors: Synthesis, Bioactivity Assessment, and Molecular Modeling. Chem Biodivers 22(11):e00974
44. Vikhrankar SS, Satbhai S, Kulkarni P, Ranbhor R, Ramakrishnan V, Kodgire P (2024) Enzymatic routes for chiral amine synthesis: protein engineering and process optimization. Targets and Therapy, Biologics, pp 165–179
45. Wang Z, Shen Y, Cao L, Li H, Li H, Song L, Ma X, Dong C (2024) Enhancing the catalytic activity of geranylgeranyl diphosphate synthase through ancestral sequence reconstruction and semirational design. J Agric Food Chem 72(34):19187–19196
46. Weng C-Y, Li J, Chen Q-L, Han J-Y, Dong Z-T, Liu Z-Q, Zheng Y-G (2025) UniESA: a unified data-driven framework for enzyme stereoselectivity and activity prediction. Green Chem 27(14):3777–3788
47. Xia T, Yu Z, Wu X, Qu J, Chen Y (2025) Catalytic reductive addition of imine for chiral amine synthesis: Recent advances and future perspectives. ChemCatChem 17(1):e202401407
48. Yao P, Marshall JR, Xu Z, Lim J, Charnock SJ, Zhu D, Turner NJ (2021) Asymmetric synthesis of N-Substituted α-amino esters from α-ketoesters via imine reductase-catalyzed reductive amination.

Angew Chem Int Ed 60(16):8717–8721

49. Ye LJ, Toh HH, Yang Y, Adams JP, Snajdrova R, Li Z (2015) Engineering of amine dehydrogenase for asymmetric reductive amination of ketone by evolving Rhodococcus phenylalanine dehydrogenase. ACS Catal 5(2):1119–1122
50. Yeh C, Hayes RL (2025) Predicting thermodynamic stability at protein G sites with deleterious mutations using λ-dynamics with competitive screening. J Phys Chem Lett 16(13):3206–3211
51. Zarifi N, Asthana P, Doustmohammadi H, Klaus C, Sanchez J, Hunt SE, Rakotoharisoa RV, Osuna S, Fraser JS, Chica RA (2025) Distal mutations enhance catalysis in designed enzymes by facilitating substrate binding and product release. Nat Commun 16(1):8662
52. Zhang Y, Liu Y, Zhang Y, Wang Z, Lu X, Ge S, Min X (2025a) Systematic evaluation of predictors for binding free energy changes upon mutations in protein complexes. Brief Bioinform 26(6):bbaf645
53. Zhang Y, Wang X, Yin X, Huang T, Lin S (2025b) Engineered ω-Transaminase Enables Remote Stereocontrol in the Synthesis of Chiral Pharmaceutical N-Heterocyclic Amines with Nonadjacent Stereocenters. ACS Catal 16(1):587–598
54. Zheng L, Zhou X-J, Jin T-Y, Ma J-L, Zhang J-W, Cai X, Liu Z-Q, Jin L-Q, Zheng Y-G (2025) Computer-aided multidimensional strategy to improve the thermostability of d-allulose 3-epimerase from christensenellaceae bacterium for the production of d-Allulose. J Agric Food Chem 73(22):13699–13709
55. Zhou L, Li C, Dong L, Liu Y, He Y, Liu G, Bai J, Ma L, Jiang Y (2024) Construction of Multi-Enzyme Integrated Catalysts for Deracemization of Cyclic Chiral Amines. ChemBioChem 25(15):e202400346
56. Zhu C, Das S, Sterling MS, Tsuji N, Léger SJ, Neese F, De CK, List B (2026) The asymmetric synthesis of an acyclic N-stereogenic amine. Nature 649(8097):621–625
57. Zhu Y-S, Xu Y, Zhu Y-Y, Huang G, Su B (2025) Enantioselective Construction of 1, 3-Stereogenic Centers via 1, 3-Borylamination of Conjugated Dienes. J Am Chem Soc 148(1):114–123

Figures

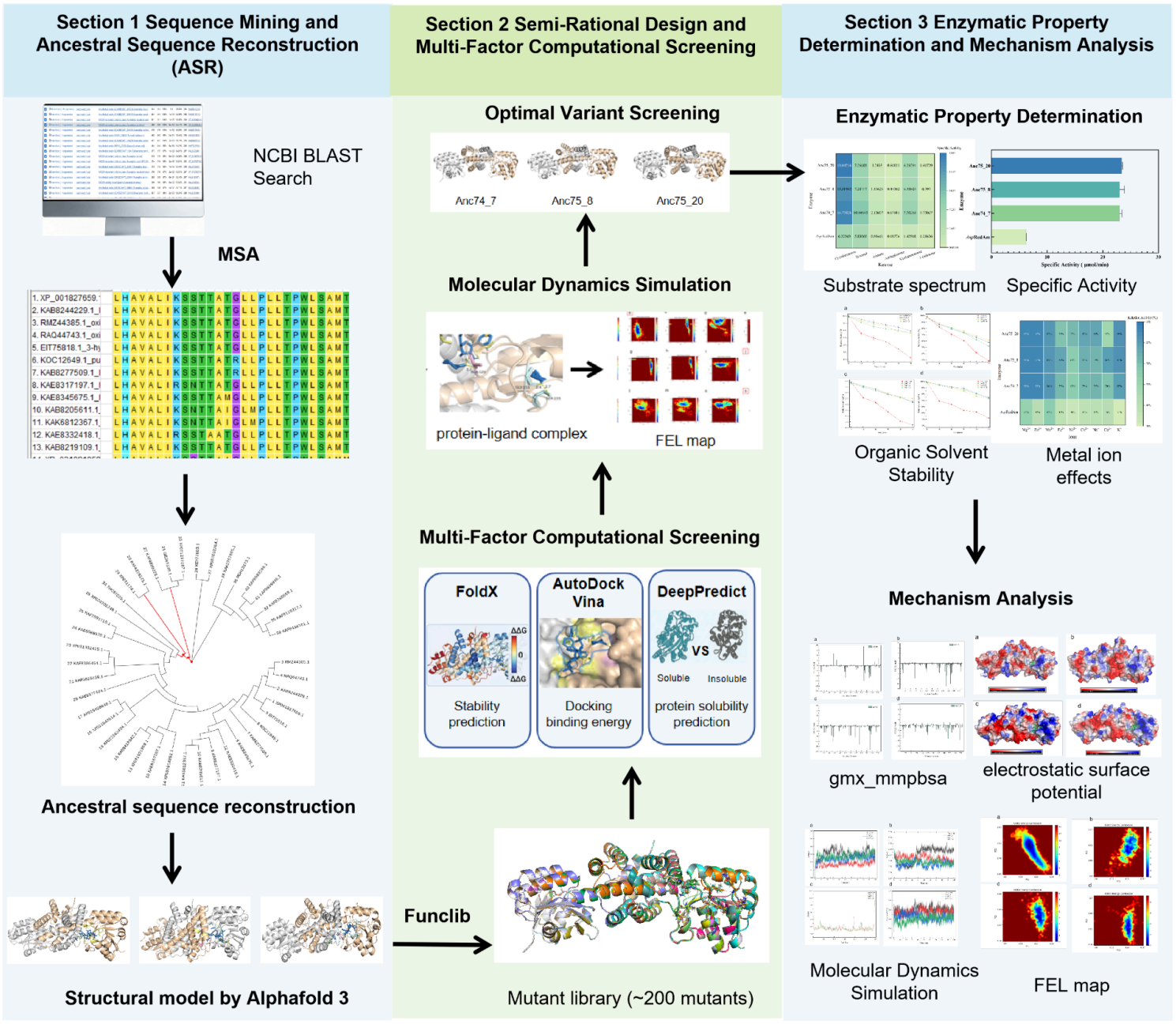


Figure 1

Diagram of the Main Research Content of this Research

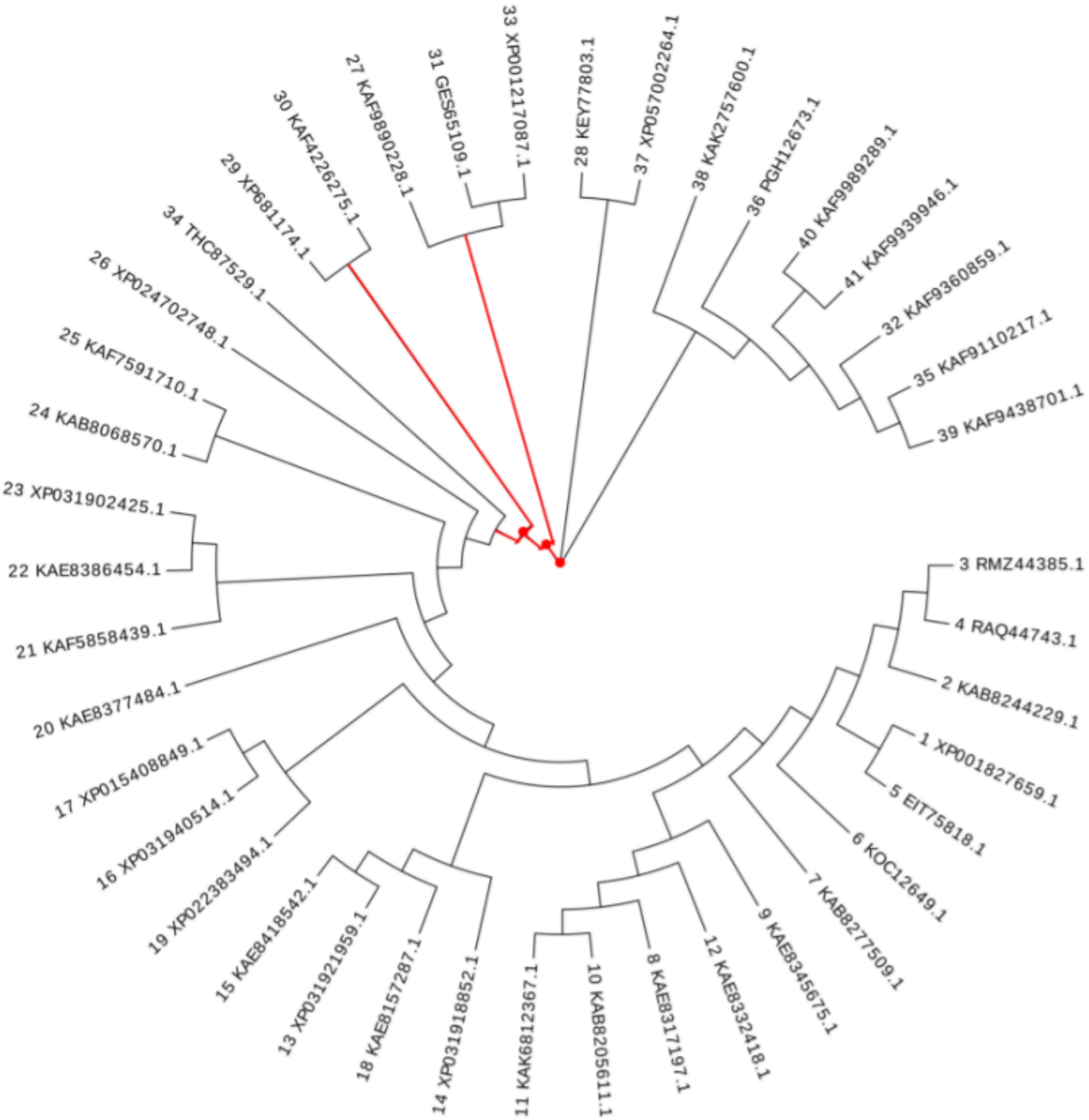


Figure 2

Ancestral Sequence Evolutionary Tree

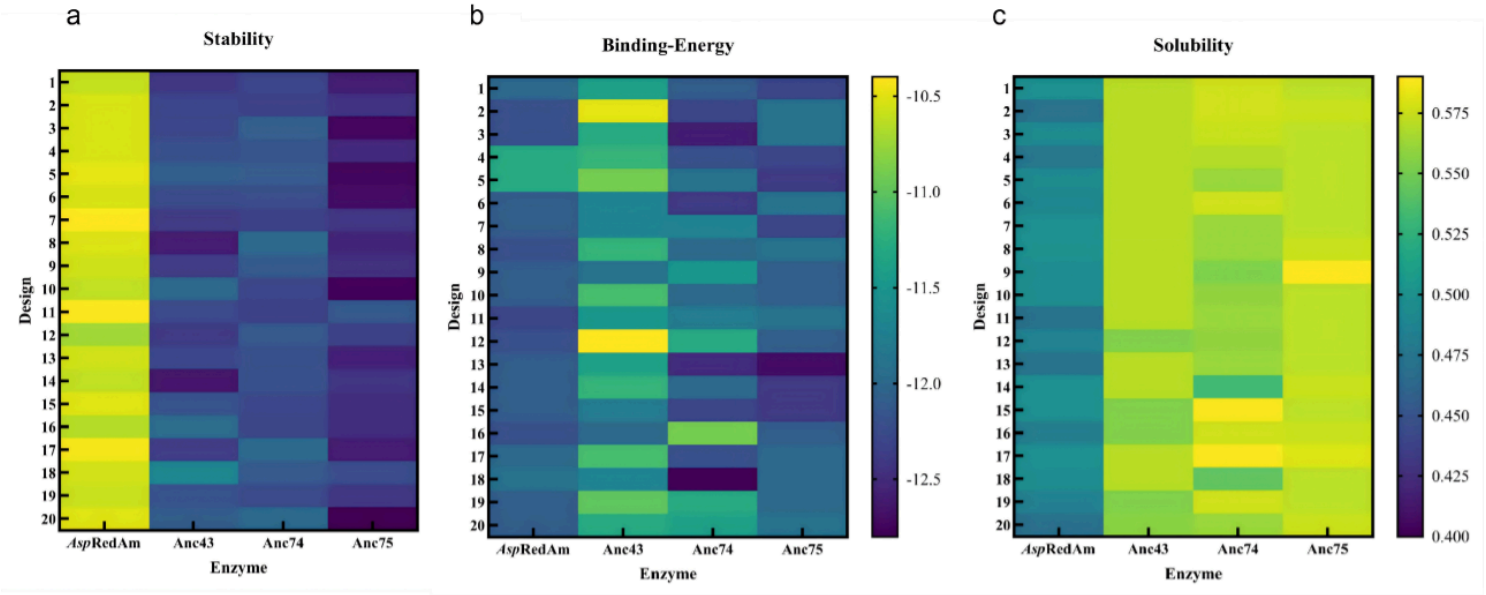


Figure 3

Screening of Mutants

Note: Performance evaluation of mutants was conducted through three *Asp*ects: stability(a) , docking binding energy(b) , and solubility(c).

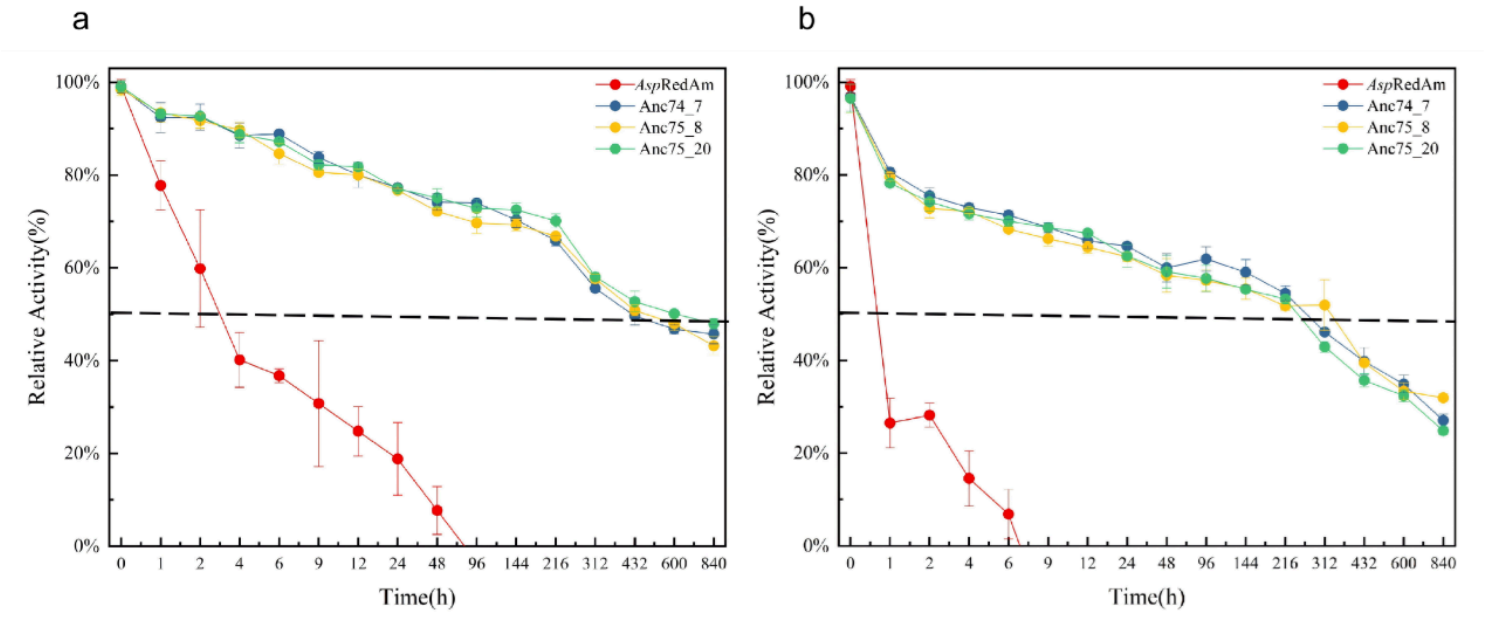


Figure 4

Half-life of *Asp*RedAm and variants

Note: (a) Half-life of *Asp*RedAm and variants at 30°C; Figure (b) Half-life of *Asp*RedAm and variants at 50°C

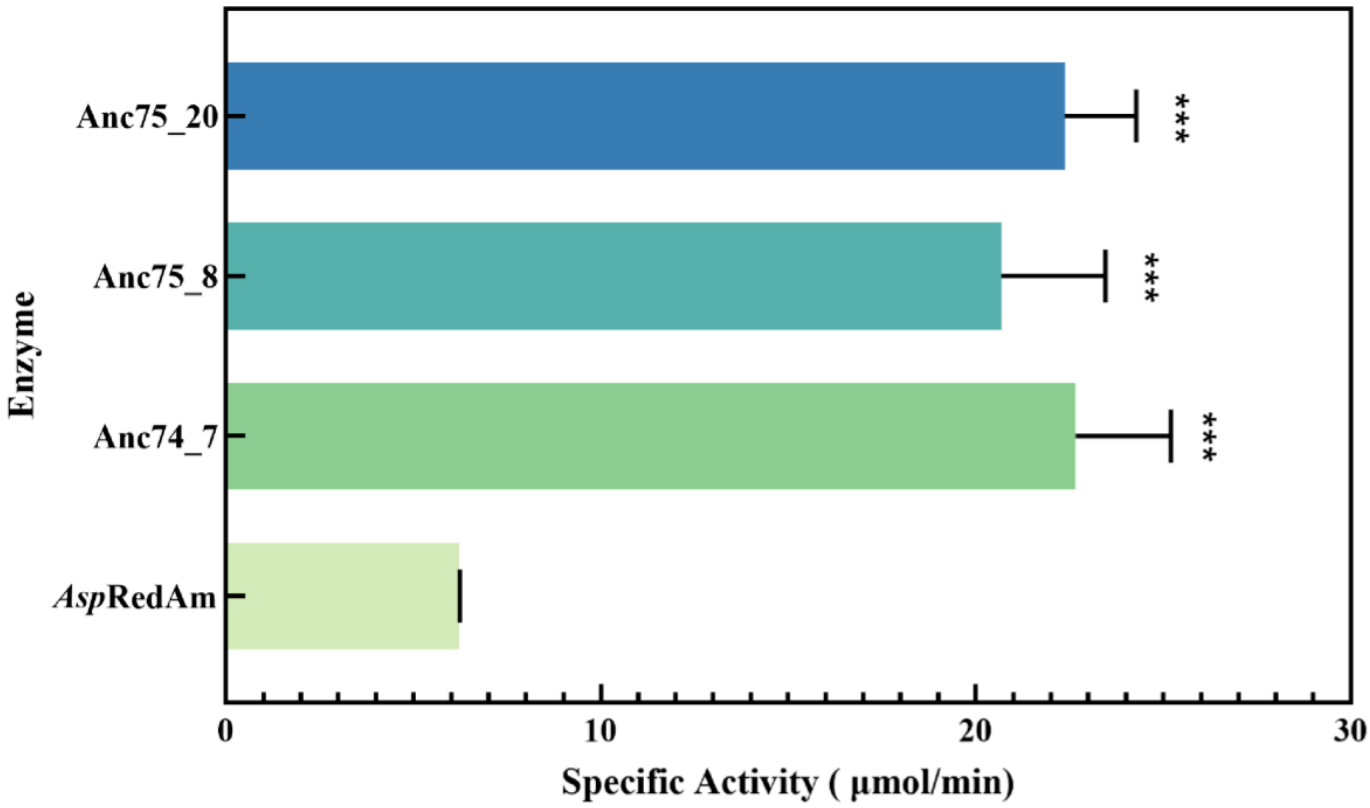


Figure 5

Specific Activity of *Asp*RedAm and variants (* indicates a significant difference from 1: 1: 1 ($p < 0.05$), ** represents a highly significant difference ($p < 0.01$), and *** represents an extremely significant difference ($p < 0.001$).)

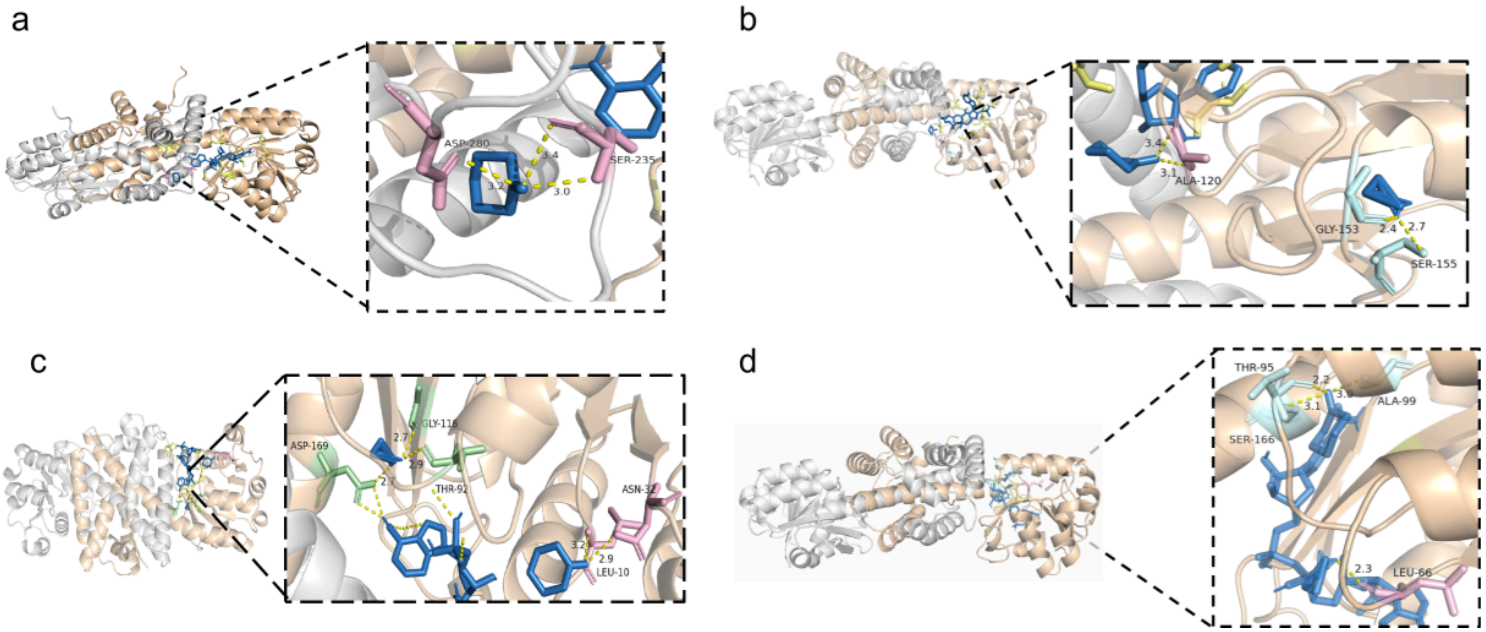


Figure 6

Molecular Docking Analysis of *Asp*RedAm and variants

Note: (a) Molecular docking analysis of *Asp*RedAm; (b) Molecular docking analysis of Anc74_4; (c) Molecular docking analysis of Anc75_8; (d) Molecular docking analysis of Anc75_20

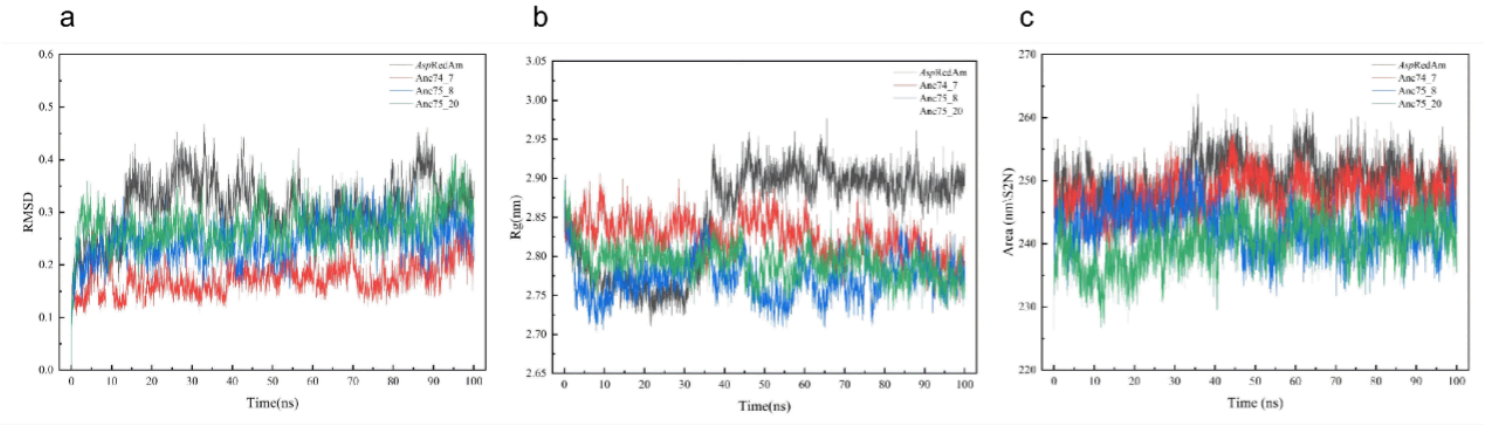


Figure 7

Molecular Dynamics Simulation Analysis of *Asp*RedAm and variants

Note: (a) RMSD analysis of *Asp*RedAm and variants; (b) Rg analysis of *Asp*RedAm and variants; (c) SASA analysis of *Asp*RedAm and variants.

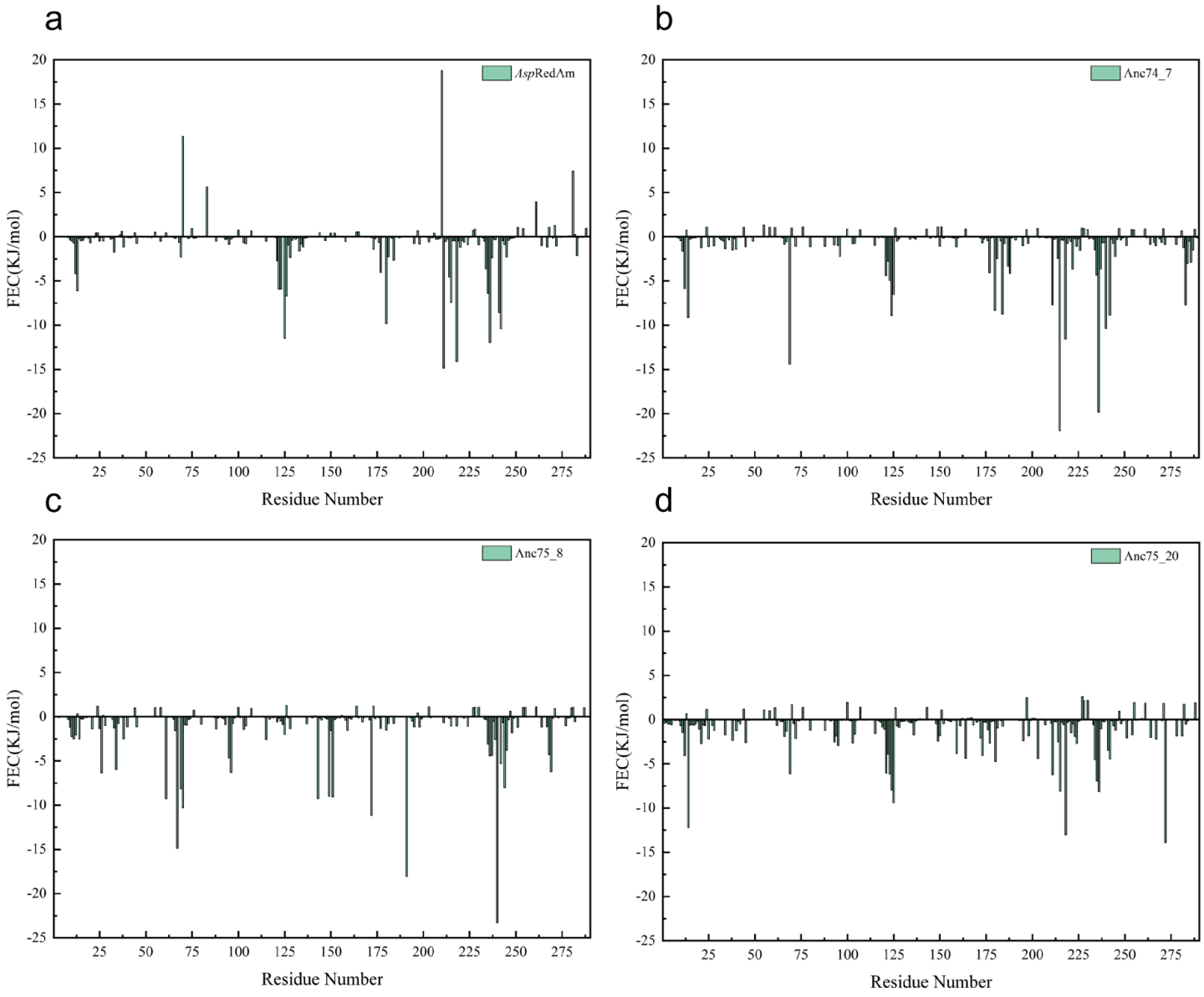


Figure 8

Residue energy contribution analysis of *Asp*RedAm and variants

Note: (a) Residue energy contribution analysis of *Asp*RedAm; (b) Residue energy contribution analysis of Anc74_7; (c) Residue energy contribution analysis of Anc75_8; (d) Residue energy contribution analysis of Anc75_20

Supplementary Files

This is a list of supplementary files associated with this preprint. Click to download.

- Supplementaryinformation.docx